
Sample Margin-Aware Recalibration of Temperature

Haolan Guo

School of Computer Science
University of Sydney
hguo4658@uni.sydney.edu.au

Linwei Tao

School of Computer Science
University of Sydney
linwei.tao@sydney.edu.au

Haoyang Luo

Department of Computer Science
City University of Hong Kong
luohaoyang.lalutte@gmail.com

Minjing Dong

School of Computer Science
University of Sydney
mdon0736@uni.sydney.edu.au

Chang Xu

School of Computer Science
University of Sydney
c.xu@sydney.edu.au

Abstract

Recent advances in deep learning have significantly improved predictive accuracy. However, modern neural networks remain systematically overconfident, posing risks for deployment in safety-critical scenarios. Current post-hoc calibration methods face a fundamental dilemma: global approaches like Temperature Scaling apply uniform adjustments across all samples, introducing high bias despite computational efficiency, while more expressive methods that operate on full logit distributions suffer from high variance due to noisy high-dimensional inputs and insufficient validation data. To address these challenges, we propose Sample Margin-Aware Recalibration of Temperature (SMART), a lightweight, data-efficient recalibration method that precisely scales logits based on the margin between the top two logits—termed the logit gap. Specifically, the logit gap serves as a denoised, scalar signal directly tied to decision boundary uncertainty, providing a robust indicator that avoids the noise inherent in high-dimensional logit spaces while preserving model prediction invariance. Meanwhile, SMART employs a novel soft-binned Expected Calibration Error (SoftECE) objective that balances model bias and variance through adaptive binning, enabling stable parameter updates even with extremely limited calibration data. Extensive evaluations across diverse datasets and architectures demonstrate that SMART achieves state-of-the-art calibration performance even with substantially fewer parameters compared to existing parametric methods, offering a principled, robust, and highly efficient solution for practical uncertainty quantification in neural network predictions. The source code is available at: <https://anonymous.open.science/r/SMART-8B11>.

1 Introduction

The deployment of deep neural networks in critical decision-making tasks requires accurate confidence estimates alongside predictions [1]. However, these models, despite high accuracy, commonly suffer from miscalibration, where predictive probabilities fail to match empirical correctness [2]. This discrepancy poses significant risks in safety-critical applications such as medical diagnosis, autonomous driving, *etc.*, where reliable uncertainty estimation is paramount.

Calibration methods can be broadly categorized into training-time approaches (*e.g.*, regularization techniques, specialized loss functions) and post-hoc methods. Post-hoc calibration offers distinct advantages: it preserves the original model’s accuracy, requires minimal computational overhead, and can be applied to any pre-trained model without retraining. Among post-hoc techniques, Temperature Scaling (TS) [1] has emerged as the standard approach due to its simplicity, applying a single global scaling factor to logits. However, TS’s uniform scaling introduces significant bias by treating all samples identically, ignoring that miscalibration varies substantially across the confidence spectrum—samples with different confidence levels often require different adjustment magnitudes. For instance, incorrect predictions typically need confidence reduction, while correct ones may benefit from confidence enhancement, a nuanced distinction that global scaling cannot capture.

To overcome these limitations, two primary strategies have been proposed. Non-parametric methods like histogram binning [3] offer better flexibility but fail to preserve prediction ordering. Alternatively, parametric approaches like Class-based Temperature Scaling (CTS) [4], vector scaling [5], and parametric temperature scaling (PTS) [6] introduce more expressive parameterizations. However, these methods face two critical challenges: First, they incorporate substantial noise by operating directly on full logit vectors or embedded features that contain irrelevant dimensions for calibration, especially in classification with a large-scale class number. Second, they employ point-wise calibration objectives that estimate model accuracy using binary dependent variables (correct or incorrect), introducing excessive variance that requires larger validation sets and model capacities to fit effectively.

Addressing these critical gaps, we introduce **SMART**, a simple yet effective calibration approach utilizing a novel indicator: the logit gap. Defined as the margin between the largest and second-largest logits, the logit gap quantifies model uncertainty at the decision boundary level. Compared with existing methods, this scalar signal replaces high-dimensional logit inputs, enabling efficient parameterization and robustness against pervasive logit noise. Theoretically, we demonstrate that the logit gap tightly bounds the optimal temperature adjustments necessary for accurate recalibration (Section 3.4), providing a principled foundation for per-sample temperature prediction. In terms of substantial variance due to the hard binning strategy [7], we adopt a SoftECE [8] as the training objective that balances bias and variance by smoothly distributing calibration errors across confidence bins. This differentiable objective enables stable gradient-based optimization even with extremely limited validation data (as few as 50 samples).

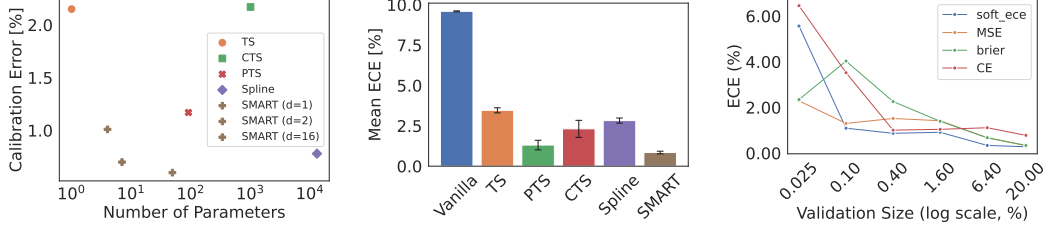
Empirically, SMART significantly outperforms baselines across various datasets and models with minimal parameters (Fig. 1a). Moreover, SMART exhibits superior stability (Fig. 1b) and shows impressive data efficiency (Fig. 1c).

Contributions Our contributions can be summarized as follows:

- We introduce the logit gap as a principled calibration indicator and implement it in our *SMART* framework. We theoretically prove that this gap tightly bounds optimal temperature adjustments and demonstrate how this enables a lightweight calibration method (down to 4 parameters) that effectively handles prediction noise while maintaining superior performance regardless of classification scale.
- We develop an efficient SoftECE training objective that optimally balances bias and variance, enabling stable parameter estimation even with extremely limited validation data (*e.g.* 50 samples), addressing a critical limitation of existing methods that depend on extensive validation sets.
- Through comprehensive evaluations against leading calibration methods, we demonstrate state-of-the-art performance across diverse architectures and datasets, with exceptional robustness under challenging domain-shift scenarios including long-tailed distributions and corrupted inputs.

2 Related Works

Non-parametric and Parametric Calibration Calibration methods can be broadly categorized into two main approaches: non-parametric and parametric techniques. Non-parametric methods offer flexibility without assuming specific functional forms, including Histogram Binning (HB) [3], which partitions confidence scores into bins, and its Bayesian extension BBQ [9]. Spline calibration [10] fits piecewise cubic functions for smooth mappings between uncalibrated and calibrated probabilities, handling sparse data regions better than isotonic regression. However, these methods often require more validation data and may alter prediction rankings. Parametric methods, in contrast, adjust model outputs through predefined functional forms. TS [1] applies a single scalar to logits, while enhanced variants include PTS [6], which uses neural networks for sample-specific temperatures, and CTS [4], which implements class-wise adjustments. Group Calibration [11] and ProCal [12] target multi-calibration [13] by grouping similar samples. Train-time approaches, including Brier Loss [14],



(a) SMART achieves lowest ECE with only 7 parameters. (b) Mean \pm std ECE across six datasets and architectures. (c) SoftECE convergence speed vs. validation set size (%).

Figure 1: (a) SMART achieves state-of-the-art ECE with extreme parameter efficiency. (b) Aggregated mean \pm std ECE over six datasets and architectures. (c) Performance vs. Validation set size (%).

Dirichlet Scaling [5], MMCE [7], Label Smoothing [15], and Focal Loss variants [16, 17], typically incur higher computational costs.

Ensemble-Based Calibration Ensemble-based calibration methods combine multiple models or outputs to approximate Bayesian inference for improved uncertainty estimation. Deep ensembles [18] provide a scalable alternative to Bayesian Neural Networks, while dropout-based approaches [19] leverage stochasticity as approximate Bayesian inference. Data-augmentation ensembles [20] improve calibration through test-time transforms, and Ensemble-based Temperature Scaling (ETS) [21] applies Bayesian principles to adjust temperatures. Though Effective, these methods typically demand significant computational resources for training multiple models or performing repeated inferences. Conversely, our approach achieves superior calibration through more efficient means.

3 Methodology

In this section, we first summarize preliminaries in Sec. 3.1. Next, we introduce a scaling adapter in Sec. 3.2 that learns to reduce calibration error using a logit gap indicator. We then analyze sample-wise objectives in Sec. 3.3 and introduce a relaxed accuracy estimation for stable temperature learning. Finally, we provide theoretical justification in Sec. 3.4.

3.1 Preliminaries

A classification model is considered *calibrated* if its predictive confidence matches its actual accuracy. Formally, for a classifier f_θ and input \mathbf{x} with true label y , perfect calibration implies $\mathbb{P}(y = \hat{y} \mid p_\theta(\hat{y} \mid \mathbf{x}) = p) = p$ for all confidence values $p \in [0, 1]$, where \hat{y} is the predicted class.

Expected Calibration Error (ECE) Consider a classification model f_θ producing logits $\mathbf{z}_i \in \mathbb{R}^K$ for a given input \mathbf{x}_i , where K is the number of classes. After applying a softmax function, we obtain the predictive probability for class k as $p_\theta(y_i = k \mid \mathbf{x}_i) = \frac{\exp(z_{i,k})}{\sum_{j=1}^K \exp(z_{i,j})}$, where $z_{i,k}$ is the k -th component of \mathbf{z}_i . To quantify calibration error, we use the *Expected Calibration Error* (ECE). In a standard binning scheme, we partition samples into B bins based on their predicted confidence, compute the average accuracy and confidence within each bin, and measure the difference. Formally, let \hat{p}_b be the average confidence and \hat{a}_b the empirical accuracy in bin b . The ECE is:

$$\text{ECE} = \sum_{b=1}^B \frac{|I_b|}{N} |\hat{p}_b - \hat{a}_b|, \quad (1)$$

where I_b is the set of indices in bin b and N is the total number of samples.

Standard Temperature Scaling Temperature scaling introduces a scalar $T > 0$ to adjust the logit distribution before the softmax:

$$p_{\theta,T}(y_i = k \mid \mathbf{x}_i) = \frac{\exp(z_{i,k}/T)}{\sum_{j=1}^K \exp(z_{i,j}/T)}. \quad (2)$$

A smaller temperature $T < 1$ sharpens the distribution, while a larger temperature $T > 1$ flattens it. Vanilla temperature scaling searches for a global \hat{T} using a held-out validation set \mathcal{D}_{val} :

$$\hat{T} = \arg \min_{T > 0} \mathcal{L}_{\text{calib}}(\mathcal{D}_{val}, f_\theta, T), \quad (3)$$

where $\mathcal{L}_{\text{calib}}$ is a chosen calibration metric such as negative log-likelihood or ECE. While effective at shifting the overall confidence distribution, a single global temperature fails to capture the *varying degrees* of miscalibration across different samples. This creates a substantial gap in achieving fine-grained calibration, as demonstrated by recent works [21, 16, 5]. This limitation has motivated various extensions, including class-wise temperature scaling [5] and parametric approaches [21], but they still do not fully leverage sample-specific calibration signals.

3.2 Scaling with Logit Gaps

Current post-hoc calibration methods face several limitations. HB and its variants often do not preserve prediction results and lack interpretability. TS applies a uniform adjustment to all samples, failing to accurately calibrate confidence at a fine-grained level. While class-wise TS and matrix scaling add flexibility, they risk altering the original model’s predictions. Recent advanced methods have explored sample-wise temperature scaling by leveraging information in embedded features or model predictions [21, 22]. However, these features were not designed specifically to provide uncertainty information but rather to assist in classification. Furthermore, for large-scale datasets with numerous classes, the increased dimensionality introduces substantial noise for precise temperature parameterization, requiring larger calibration sample sets. The crucial problem is: how can we precisely scale the output logits for calibration, while maintaining the invariance in model prediction? Aiming at this goal, we propose to leverage a *single scalar* as a denoised signal from the logit space of possibly thousands of classes. Specifically, let

$$z_{i,\max} = \max_{k \in [K]} z_{i,k}, \quad z_{i,2\text{nd}} = \max_{k \in [K] \setminus \{\arg \max_k z_{i,k}\}} z_{i,k} \quad (4)$$

Then we define the **logit gap** for sample i as

$$g_i = z_{i,\max} - z_{i,2\text{nd}}. \quad (5)$$

Intuitively, a model generally exhibits higher confidence in a specific sample when there exists a substantial gap between the largest and the second-largest logits. Conversely, smaller logit gaps indicate greater uncertainty for harder samples that possibly require different confidence adjustments. Unlike high-dimensional embeddings or complex uncertainty proxies, this simple measure directly arises from the classifier’s decision boundary and naturally reflects prediction stability. It is worth noting that the predicted confidence or the maximum logit themselves cannot indicate such knowledge, as they only carry intra-class signals.

Light-weight Temperature Regression While current approaches emphasize on network expressiveness [6] to capture complex patterns in mapping the full logit distributions to temperature shifts, they become over-parameterized for processing the proposed logit gaps, as the learned scalar-to-scalar relationship is simple and direct. Aiming at devising a minimal but precise parameterization design, we model temperature regression $h_\phi(\cdot) : \mathbb{R} \rightarrow \mathbb{R}$ as a single hidden layer MLP, *i.e.*,

$$\hat{T} = h_\phi(g_i) = \text{softplus}(\mathbf{W}_2 \cdot \text{ReLU}(\mathbf{W}_1 \cdot g_i + \mathbf{b}_1) + b_2) + \epsilon, \quad (6)$$

where $\mathbf{W}_1 \in \mathbb{R}^{d \times 1}$, $\mathbf{W}_2 \in \mathbb{R}^{1 \times d}$, $\mathbf{b}_1 \in \mathbb{R}^d$, and $b_2 \in \mathbb{R}$ are learnable parameters and the hidden dimension d is set to 16 in our implementation. The softplus activation and $\epsilon = 10^{-6}$ ensure positive temperatures with numerical stability. Though simple, such a restrained design is built on the fact that a desired temperature value T_i is tightly bounded by g_i as analyzed in Sec. 3.4 theoretically. Our parameterization enables effective temperature adjustment with substantially fewer parameters of a fixed $3d + 1 = 49$ values, while the parameter size of PTS [6] (two hidden layers of size 5 on the top-10 logits) is a fixed 91 values [6], CTS [1] learns C temperatures, vector scaling [5] uses $2C$ parameters, matrix scaling or Dirichlet calibration [5] incur $C^2 + C$ parameters, and Spline [10] results in $13C$ parameters. For ImageNet ($C = 1,000$), these latter approaches become ill-shaped and inefficient to learn precise confidence adjustments.

3.3 Precise Temperature Mapping with Soft-Bin ECE

Current post-hoc calibration methods face a fundamental bias-variance tradeoff: they either use global objectives with minimal parameterization (high bias) or point-wise objectives that introduce substantial variance through binary-valued dependent variables. Following [23], we reformulate the problem as regression of model accuracy given confidence distribution:

$$\min_{\phi} \int \|\hat{p} - \mathbb{E}_{\hat{p}}^{\text{acc}}\| dp(\hat{p}) = \int \left\| \hat{p} - \int \mathbb{I}\{y_{\mathbf{x}} = \hat{y}_{\mathbf{x}}\} dp(\mathbf{x}|\hat{p}) \right\| dp(\hat{p}), \quad (7)$$

Due to intractable distributions $p(\mathbf{x}|\hat{p})$, existing methods rely on approximations. Global methods use overall accuracy $\mathbb{E}^{\text{global}} = \frac{1}{N} \sum_{i=1}^N \mathbb{I}\{y_i = \hat{y}_i\}$, introducing substantial bias while permitting only minimal parameterization. In contrast, sample-wise methods [6, 23] use point-level approximation $\mathbb{E}_{\hat{x}_i}^{\text{point}} = \mathbb{I}\{y_i = \hat{y}_i\}$, which introduces high variance from binary-valued dependent variables, necessitating heavier parameterization.

To balance bias and variance, we divide the confidence space using range-wise discrete bins with a membership function:

$$P(b|\hat{p}_i) = w_{i,b} = \frac{\exp(-\alpha(\hat{p}_i - c_b)^2)}{\sum_{b'=1}^B \exp(-\alpha(\hat{p}_i - c_{b'})^2)}, \quad (8)$$

where c_b is the bin center and $\alpha > 0$ controls weighting smoothness. The estimated model accuracy per bin becomes:

$$\mathbb{E}_b^{\text{soft}} = \sum_{i=1}^N w_{i,b} \mathbb{I}\{y_i = \hat{y}_i\} / \sum_{i=1}^N w_{i,b}. \quad (9)$$

Notably, as $\alpha \rightarrow 0^+$, $\mathbb{E}_b^{\text{soft}}$ degenerates to $\mathbb{E}^{\text{global}}$, while setting $b \rightarrow 0$ produces $\mathbb{E}_{\hat{x}_i}^{\text{point}}$. Thus, α and b serve as natural bias-variance knobs, enabling both parameter efficiency and precise confidence estimation. This approach distributes each prediction’s influence across neighboring bins, creating smooth gradients throughout the confidence spectrum and yielding the soft-binned ECE [8] objective:

$$\text{SoftECE}(\mathcal{D}_{\text{val}}, \theta) = \left(\sum_{b=1}^B \frac{\sum_{i=1}^N w_{i,b}}{N} \left| \mathbb{E}_{\hat{p}}^{\text{soft}} - \frac{\sum_{i=1}^N w_{i,b} \hat{p}_i}{\sum_{i=1}^N w_{i,b}} \right|^q \right)^{1/q}, \quad (10)$$

Figure 1(a, c) demonstrates SoftECE’s superior performance across varying parameter counts and validation set sizes, maintaining its advantage even with just 0.1% of the dataset for validation. As shown in Section 4.5, this balanced approach delivers consistent performance across diverse architectures and datasets. Algorithm in Appendix C details our implementation.

3.4 Theoretical Evidence for Logit Gaps

We theoretically explain the choice of logit gap g_i as the prediction output’s scalar proxy. Despite the direct scaling effect caused by temperature adjustments, the essence of post-hoc calibration actually lies in precisely controlling the confidence values. Given a specific target confidence, we argue that the maximum logit, despite indicating the confidence before scaling, can hardly bound the best temperature. As a contrast, the devised indicator of logit gap can effectively make a tight bound of such temperature values. Specifically, given a target confidence value \hat{p} , the parameterization model and the soft-ECE objective aims to search a temperature value T subject to

$$\frac{\exp(z_{\max}/T)}{\sum_{j=1}^K \exp(z_j/T)} = \hat{p}, \quad (11)$$

where we assume $\hat{p} \in (0, 1)$ is a fixed value (e.g., 0.82) determined by minimizing our Soft-ECE objective for each sample \mathbf{z} . The sample index subscript is omitted here and subsequently for brevity. The logit gap’s theoretical superiority in confidence adjustment is demonstrated by two propositions:

Proposition 3.1 (Unbounded Temperature). *The implicit function $T = \beta(\mathbf{z})$ defined by Eq. (11) is unbounded when fixing z_{\max} , with T taking values in $(0, +\infty)$.*

Proposition 3.2 (g -Boundedness). *T is bounded by $-g/\log(\frac{1-\hat{p}}{\hat{p}}) < T \leq -g/\log(\frac{1-\hat{p}}{\hat{p}(n-1)})$.*

Therefore, when $\hat{p} > 0.5$, which takes up most cases, our proposed logit gap indicator can effectively determine the temperature when receiving gradients for altering the confidence. A numerical verification is illustrated in Fig. 2, where logit gaps outperform other scalar indicators (a-c) and facilitate both convergence and performance compared to full logit values (d), statistically validating the superiority of logit gaps in indicating the temperature adjustment. Full proofs are in Appendix A.

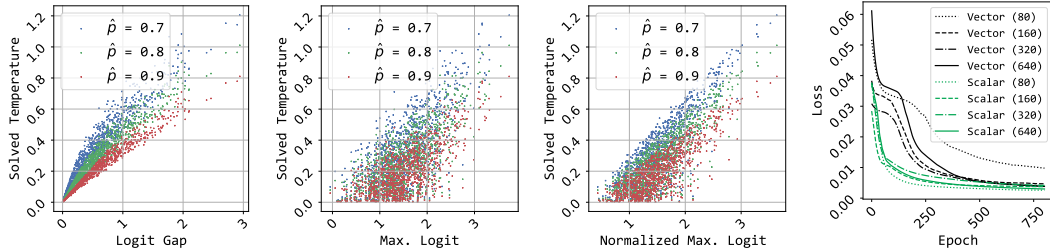


Figure 2: **Numerical study of temperature adjustment indicators.** The left 3 plots: Joint distribution of the solved T and multiple indicators across 1,000 logit data points. The right plot: MSE loss curves for confidence adjustment to a fixed value of $\hat{p} = 0.8$, comparing vector (sorted logits) and scalar (logit gaps) approaches with varying validation sizes (bracketed) and a fixed number of 193 parameters.

4 Experiments

4.1 Experimental Setup

Datasets We conduct experiments on several benchmark datasets, including CIFAR-10, CIFAR-100 [24], and ImageNet [25]. To probe robustness under common corruptions and distribution shifts, we include *ImageNet-C* (All corruption type averaged, severity 5) [26], *ImageNet-LT* (a long-tailed variant with power-law class imbalance) [27], and *ImageNet-Sketch* (sketch-based OOD variant) [28]. All experiments employ a training-time batch size of 1024. CIFAR-10 and CIFAR-100 contain 60,000 images of size 32×32 pixels, with 10 and 100 classes, respectively, split into 45,000 training, 5,000 for validation and 10,000 test images. For ImageNet related dataset, we use only 50 sample, 0.001 of the original validation set, as the new validation set, with the remainder used as the test set. The testing batch size for all datasets is set to 128.

Model Architectures. To demonstrate the generality of our calibration methods, we evaluate across a diverse collection of convolutional and transformer-based networks. For CIFAR-10 and CIFAR-100, we employ ResNet-50 and ResNet-110 [29], Wide-ResNet [30], and DenseNet-121 [31], initialized with pretrained weights from Mukhoti *et al.* [32]. Each model is trained for 350 epochs using stochastic gradient descent with momentum 0.9, weight decay 5×10^{-4} , and a piecewise-constant learning-rate schedule ($0.1 \rightarrow 0.01 \rightarrow 0.001$ over 150/100/100 epochs). ImageNet and its variants are evaluated on PyTorch’s pretrained ResNet-50 and DenseNet-121 [33], the transformer designs Swin-B [34], ViT-B/16 and ViT-B/32 [35], and Wide-ResNet-50. This suite spans from compact CNNs to large-capacity transformers, allowing us to assess calibration robustness under varying architectural inductive biases and model complexities. Calibration performance is primarily evaluated using ECE, with additional metrics including AdaECE and top-1 accuracy. All experiments are conducted on a NVIDIA 3090 GPU, with results averaged over five seeds to ensure fairness.

4.2 Calibration Performance

We evaluate SMART against leading post-hoc calibration approaches including TS [1], PTS [6], CTS [36], and spline-based calibration [10], as well as uncalibrated (Vanilla) models across both standard settings and distribution shift scenarios.

Calibration on Standard Datasets SMART consistently outperforms these methods across CIFAR10, CIFAR-100, and ImageNet-1K (Table 1), significantly reducing calibration error. The most notable improvement is seen in CIFAR-100, where SMART excels while Spline, despite its strong performance on other datasets, struggles. This highlights SMART’s robustness across datasets with varying complexities. CNNs, which often suffer from overconfidence, are generally well-calibrated with TS-based methods. However, transformers see limited calibration improvements from TS-based methods, with SMART outperforming them by a large margin. On larger datasets like ImageNet-1K, SMART maintains its advantage with consistently lower ECE values. While Spline achieves competitive performance on some model configurations (e.g., slightly outperforming SMART on ViT-B-32), it exhibits substantially higher variance across different seeds, indicating lower stability compared to our method. This instability stems from Spline’s over-parameterization, further discussed in Section 3.2, where its 13C parameters become unwieldy for datasets with large class counts. In contrast, SMART’s lightweight parameterization with only 49 parameters consistently delivers both strong performance and stability.

Table 1: **Comparison of Post-Hoc Calibration Methods Using ECE(\downarrow , %, 15bins) Across Various Datasets and Models (5 Seeds Averaged).** The best-performing method for each dataset-model combination is in bold, and our method (SMART) is highlighted.

Dataset	Model	Vanilla	TS	PTS	CTS	Spline	SMART (ours)
CIFAR-10	ResNet-50	4.34 \pm 0.0%	1.38 \pm 19.0%	1.10 \pm 18.9%	0.83 \pm 17.5%	1.52 \pm 2.1%	0.85 \pm 2.8%
	Wide-ResNet	3.24 \pm 0.0%	0.93 \pm 21.5%	0.90 \pm 21.5%	0.81 \pm 21.0%	1.74 \pm 0.3%	0.43 \pm 11.6%
CIFAR-100	ResNet-50	17.53 \pm 0.0%	5.61 \pm 24.7%	1.96 \pm 24.7%	3.67 \pm 24.0%	3.48 \pm 0.0%	1.37 \pm 19.9%
	Wide-ResNet	15.34 \pm 0.0%	4.50 \pm 13.8%	1.96 \pm 13.8%	3.01 \pm 14.0%	3.76 \pm 0.1%	1.80 \pm 5.7%
ImageNet-1K	ResNet-50	3.65 \pm 1.1%	2.17 \pm 1.3%	0.95 \pm 38.0%	2.17 \pm 36.0%	0.62 \pm 28.7%	0.61 \pm 19.6%
	DenseNet-121	2.53 \pm 1.0%	1.85 \pm 1.9%	1.02 \pm 45.3%	1.86 \pm 43.5%	0.81 \pm 43.0%	0.61 \pm 5.3%
	Wide-ResNet	5.43 \pm 0.4%	2.89 \pm 3.7%	1.14 \pm 21.3%	3.27 \pm 21.0%	0.66 \pm 15.8%	0.52 \pm 12.5%
	Swin-B	5.06 \pm 0.5%	3.91 \pm 1.9%	1.05 \pm 4.6%	1.53 \pm 5.0%	0.88 \pm 16.2%	0.63 \pm 5.2%
	ViT-B-16	5.60 \pm 1.1%	3.60 \pm 5.4%	1.23 \pm 23.9%	4.65 \pm 22.0%	0.91 \pm 34.1%	0.86 \pm 15.4%
	ViT-B-32	6.41 \pm 0.4%	3.93 \pm 0.6%	1.27 \pm 76.0%	2.12 \pm 75.0%	0.81 \pm 14.5%	0.87 \pm 21.1%
ImageNet-C	ResNet-50	13.84 \pm 0.2%	1.97 \pm 1.2%	1.12 \pm 11.5%	1.69 \pm 12.0%	5.61 \pm 2.6%	0.68 \pm 4.6%
	DenseNet-121	12.58 \pm 0.1%	1.58 \pm 0.2%	1.19 \pm 12.4%	1.44 \pm 13.0%	5.18 \pm 2.5%	0.63 \pm 1.9%
	Swin-B	11.98 \pm 0.2%	5.82 \pm 0.9%	1.53 \pm 0.0%	3.05 \pm 0.2%	2.58 \pm 8.0%	1.23 \pm 3.4%
	ViT-B-16	8.24 \pm 0.1%	5.24 \pm 0.1%	1.27 \pm 3.6%	2.76 \pm 3.8%	1.71 \pm 12.8%	1.06 \pm 2.3%
	ViT-B-32	7.68 \pm 0.2%	5.10 \pm 0.0%	1.07 \pm 7.3%	2.97 \pm 8.0%	1.43 \pm 17.1%	0.99 \pm 1.5%
ImageNet-LT	ResNet-50	3.63 \pm 0.3%	2.01 \pm 1.1%	0.99 \pm 32.0%	2.17 \pm 31.5%	0.56 \pm 18.1%	0.56 \pm 7.1%
	DenseNet-121	2.51 \pm 2.6%	1.80 \pm 3.1%	1.20 \pm 21.9%	1.88 \pm 22.0%	0.79 \pm 8.7%	0.81 \pm 1.5%
	Wide-ResNet	5.40 \pm 0.2%	2.99 \pm 1.6%	1.21 \pm 63.4%	2.87 \pm 62.5%	0.81 \pm 29.5%	0.53 \pm 4.0%
	Swin-B	4.70 \pm 0.9%	3.98 \pm 3.1%	1.21 \pm 36.9%	1.50 \pm 37.0%	0.79 \pm 21.0%	0.66 \pm 1.2%
	ViT-B-16	5.58 \pm 0.8%	3.73 \pm 3.5%	1.14 \pm 41.2%	1.43 \pm 40.5%	0.66 \pm 8.1%	0.56 \pm 25.6%
	ViT-B-32	6.26 \pm 0.6%	3.98 \pm 1.5%	1.35 \pm 30.3%	2.12 \pm 29.5%	0.72 \pm 31.8%	0.79 \pm 13.8%
ImageNet-S	ResNet-50	22.31 \pm 0.3%	2.06 \pm 2.7%	1.69 \pm 16.0%	1.48 \pm 15.5%	9.76 \pm 2.3%	0.92 \pm 10.0%
	DenseNet-121	20.15 \pm 0.5%	1.67 \pm 17.0%	1.93 \pm 9.6%	1.16 \pm 9.3%	9.20 \pm 3.5%	0.76 \pm 32.3%
	Swin-B	24.62 \pm 0.0%	6.50 \pm 0.7%	1.53 \pm 12.2%	3.62 \pm 12.5%	8.66 \pm 1.7%	1.42 \pm 3.8%
	ViT-B-16	16.57 \pm 0.2%	5.75 \pm 1.4%	1.33 \pm 15.7%	2.84 \pm 15.0%	5.70 \pm 3.3%	0.98 \pm 8.4%
	ViT-B-32	14.19 \pm 0.3%	4.99 \pm 3.0%	1.67 \pm 16.1%	3.25 \pm 15.5%	4.07 \pm 5.1%	0.87 \pm 21.0%

Robustness under Class Imbalance and Distribution Shift Across long-tailed (ImageNet-LT) and corrupted scenarios (ImageNet-Sketch, ImageNet-C), SMART’s sample-wise temperature adaptation consistently outperforms global and class-wise scalars. Uniform approaches such as TS and PTS struggle to accommodate underrepresented classes or severe input degradations, leading to pronounced calibration drift. Notably, PTS exhibits very high variance, confirming our analysis in Section 3.2 that high-dimensional parameterizations introduce substantial noise for precise temperature estimation, particularly on complex datasets. Furthermore, CTS mitigates some class imbalance but incurs uneven per-class adjustments and high computational cost, similar to PTS, due to its C parameters growing linearly with class count. These methods all suffer from the fundamental limitation we identified—they lack an effective, low-dimensional signal for calibration that preserves model prediction invariance.

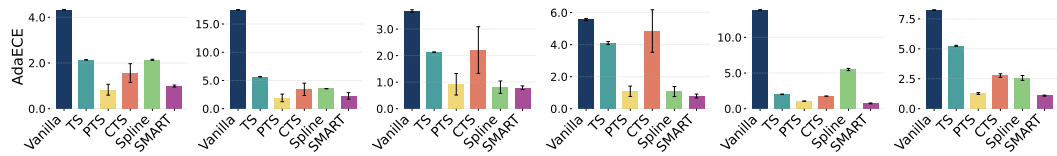


Figure 3: **Comparison of calibration methods using AdaECE \downarrow across various datasets and models.** From left to right: CIFAR-10 (ResNet-50), CIFAR-100 (ResNet-50), ImageNet (ResNet-50), ImageNet (ViT-B-16), ImageNet-C (ResNet-50), and ImageNet-C (ViT-B-16). Results are averaged.

Calibration Performance on AdaECE We also evaluate SMART using Adaptive Expected Calibration Error (AdaECE) to provide a comprehensive view of its performance, shown in Figure 3, with additional results available in Appendix D. SMART demonstrates superior performance on AdaECE compared to traditional calibration methods across diverse settings. AdaECE addresses limitations of standard ECE by accounting for uneven confidence distributions, providing a more reliable measure of calibration quality. SMART consistently achieves the lowest AdaECE values and variance across CNN and ViT architectures and datasets (CIFAR and ImageNet variants), demonstrating its robustness to dataset shifts and model architectures. Notably, SMART outperforms more complex methods like Spline calibration and CTS in calibration error and variance while requiring fewer parameters.

By leveraging instance-level temperature through logit gaps, SMART yields stable calibration gains across diverse distribution shifts. Its lightweight per-sample inference preserves efficiency while delivering robustness that neither fixed nor ensemble temperature schemes can match. In contrast, Spline collapses on particularly challenging shifts such as ImageNet-S and ImageNet-C — whereas our method consistently sustains the lowest and most stable calibration error even under these adverse conditions.

4.3 Comparison With Training-Time Calibration Methods

We evaluate SMART alongside training-time calibration techniques in Table 2, including Brier Loss [14], Maximum Mean Calibration Error (MMCE) [7], Label Smoothing (LS-0.05) [15], and Focal Loss variants (FLSD-53 and FL-3) [16]. This shows that combining SMART with these methods consistently enhances calibration performance across various models and datasets, further validating SMART’s effectiveness alongside training-time approaches. Moreover, as seen in Table 1, SMART alone, as a post-hoc calibration method, already outperforms these train-time techniques with minimal computational overhead, while train-time methods require significantly more resources.

Table 2: **Comparison of Train-time Calibration Methods Using ECE(↓, %, 15 bins) Across Various Datasets and Models.** The best-performing method for each dataset-model combination is in bold, and our method (SMART) is highlighted. Results are averaged over 5 runs.

Dataset	Model	Cross-Entropy		Brier Loss		MMCE		LS-0.05		FLSD-53		FL-3	
		base	ours	base	ours	base	ours	base	ours	base	ours	base	ours
CIFAR10	ResNet-50	4.34	0.75	1.81	0.96	4.57	0.53	2.97	0.51	1.56	0.42	1.47	0.43
	ResNet-110	4.41	0.44	2.56	0.60	5.07	0.38	2.09	0.28	1.87	0.45	1.54	0.54
	DenseNet-121	4.51	0.53	1.52	0.31	5.10	0.66	1.89	0.51	1.23	0.62	1.31	1.02
	Wide-ResNet	3.24	0.30	1.25	0.38	3.30	0.34	4.25	0.36	1.58	0.39	1.68	0.54
CIFAR100	ResNet-50	17.53	0.99	6.54	1.01	15.31	0.86	7.81	1.50	4.49	1.26	5.16	0.56
	ResNet-110	19.06	0.98	7.87	0.87	19.13	1.42	11.03	1.01	8.54	0.85	8.65	0.73
	DenseNet-121	20.99	1.86	5.22	0.59	19.10	1.34	12.87	1.02	3.70	0.91	4.14	0.98
	Wide-ResNet	15.34	1.38	4.35	1.00	13.17	0.98	4.88	1.24	3.02	0.79	2.14	1.12

4.4 SMART is Data Efficient

Data Efficiency SMART exhibits exceptional data efficiency, maintaining low calibration error even with minimal validation data. We compared SMART against TS, PTS, and Spline across varying validation set sizes (0.001% to 11%) on both ImageNet (ResNet-50) and its corrupted variant ImageNet-C (Figure 4). While TS maintains a relatively flat ECE curve across all validation sizes, confirming its baseline robustness to data scarcity, more expressive methods show different behaviors. PTS demonstrates sensitivity to limited samples, with ECE increasing noticeably below 10% validation size as its neural network struggles to learn reliable mappings with insufficient examples. Spline shows moderate degradation with decreasing validation data. In contrast, SMART’s use of the logit gap—a succinct, high-signal measure of sample uncertainty—enables stable temperature estimation even with extremely limited data. This advantage is particularly evident in the challenging ImageNet-C setting, where TS and PTS suffer pronounced ECE spikes (especially around 3% validation size), while SMART consistently maintains low calibration error, demonstrating superior stability in data-constrained and distribution-shifted scenarios.

Bin-Size Sensitivity Figure 4 (right) illustrates the mean ECE across the 6 architectures trained on ImageNet and calibrated using TS, PTS, Spline and SMART. While small bin sizes result in a systematically smaller ECE - a known bias [37] - SMART outperforms the other TS-based methods and Spline for all bin sizes with rankings being unchanged.

Runtime Efficiency To verify the time efficiency of our method, we compare the inference time with baseline methods. The result is reported in Table 3. TS optimizes a single scalar temperature via

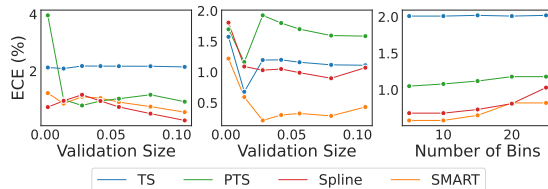


Figure 4: **ECE(↓, %, 15 bins) w.r.t. validation-set size and bin count.** (Left) In-distribution calibration on ImageNet (ResNet-50); (Middle) OOD calibration on ImageNet-C (Gaussian Noise, s=5; ResNet-50); (Right) Bin-size sensitivity of ECE on ImageNet (ResNet-50). We compare TS, PTS, Spline and SMART. Curves are averaged over five runs.

Table 3: **Average Runtime (s) on ImageNet** over 10 runs on a ResNet-50 model.

Method	TS	Spline	PTS	CTS	SMART
Runtime (s)	$2.42 \pm 5.8\%$	$28.51 \pm 3.1\%$	$90.44 \pm 3.6\%$	$5457.55 \pm 2.3\%$	$23.03 \pm 1.8\%$

Table 4: **Ablation study for different losses** reported in ECE(\downarrow , %, 15 bins) on ImageNet-1K.

Architecture	Method	CE	LS	MSE	Brier	Soft-ECE
ResNet-50 (Top-1=0.761)	TS	$2.04 \pm 1.5\%$	$14.33 \pm 0.8\%$	$3.69 \pm 1.4\%$	$2.31 \pm 1.7\%$	$3.16 \pm 1.9\%$
	PTS	$1.04 \pm 3.8\%$	$1.87 \pm 2.7\%$	$1.89 \pm 1.6\%$	$1.88 \pm 2.1\%$	$1.88 \pm 2.7\%$
	SMART	$0.93 \pm 2.2\%$	$1.09 \pm 2.8\%$	$1.39 \pm 1.4\%$	$1.38 \pm 1.4\%$	$0.65 \pm 1.5\%$
ViT-B/16 (Top-1=0.810)	TS	$3.73 \pm 1.3\%$	$6.05 \pm 1.7\%$	$5.58 \pm 1.4\%$	$3.11 \pm 1.3\%$	$3.10 \pm 1.6\%$
	PTS	$5.69 \pm 3.5\%$	$3.22 \pm 1.6\%$	$2.40 \pm 1.7\%$	$2.57 \pm 1.9\%$	$1.15 \pm 1.7\%$
	SMART	$3.62 \pm 1.7\%$	$3.11 \pm 2.3\%$	$0.84 \pm 1.2\%$	$0.80 \pm 1.3\%$	$0.89 \pm 2.2\%$

a few gradient steps or closed-form updates, then applies this same factor to every logit, resulting in a negligible overhead (2.42 s). SMART yields a small per-sample inference cost and hence a modest total runtime (23.03 s). Logits are input into PTS’s small neural network for each sample to predict a bespoke temperature, incurring a larger computational cost than SMART. CTS is the most expensive at more than 1 hour with the highest variance, as it conducts an exhaustive grid search for 5 epoches over a dense temperature grid (e.g. 0.1 -10) for each of the 1 000 classes, leading to $O(C \times G \times N)$ evaluations (classes \times grid points \times samples). The spline-based calibrator precomputes a monotonic mapping on the validation set and then applies a fast piecewise-linear transform at test time, yielding intermediate overhead. These differences illustrate the trade-off between expressive power and efficiency: TS is almost instantaneous, SMART adds only a small network-forward cost per sample, PTS trades per-sample flexibility for moderate cost, and CTS’s brute-force search becomes prohibitive at scale.

4.5 Ablation Studies

Choice of Loss Our comprehensive analysis reveals fundamental differences in how various loss functions influence SMART’s calibration performance. While all tested losses enable significant improvements over uncalibrated baselines, they exhibit distinct behavior patterns across architectures. Cross-entropy and label smoothing losses, despite their prevalence in classification tasks, demonstrate suboptimal calibration performance due to their indirect relationship with confidence estimation objectives. MSE and Brier score offer more reliable improvements by directly penalizing squared confidence errors, yet their effectiveness fluctuates between CNN and transformer architectures. Soft-ECE emerges as the superior choice by directly optimizing the calibration metric itself, achieving both the lowest average error and the smallest variance across diverse model architectures, making it the most stable choice for SMART’s temperature mapping.

Table 5: **Ablation study on alternative inputs** for temperature network on ImageNet-1K dataset.

Model	Entropy	Conf.	All Logits	Logit _{max}	Logit _{max} - Logits	Logit Gap (ours)
ResNet-50	0.87	0.97	0.87	0.91	0.85	0.58
DenseNet-121	0.62	0.89	0.79	0.80	0.84	0.56
Wide-ResNet	1.00	1.22	0.92	0.57	0.63	0.52
Swin-B	0.62	0.81	0.89	0.78	0.87	0.63
ViT-B/16	0.90	0.75	0.97	0.91	1.20	0.72

Choice of Indicators We conduct an ablation study on ImageNet-1K to compare six candidate uncertainty signals as inputs to our temperature network (Table 5): predictive entropy $H(\mathbf{z})$, logit margin ($z_{\max} - z_{2\text{nd}}$), the full logit vector \mathbf{z} , maximum logit $\max_c z_c$, mean-normalized logit deviation $\max_c z_c - \frac{1}{C} \sum_c z_c$, direct predicted confidence $p_{\max} = \max_c \text{softmax}(z_c)$, and our logit gap g_i . The logit gap consistently outperforms alternative uncertainty indicators across all tested architectures by capturing decision boundary information in its most essential form. Full logit vectors, despite their richness, introduce excessive noise that degrades performance in limited-data scenarios, while simpler scalar indicators like maximum logit or predicted confidence fail to adequately represent class competition dynamics. Predictive entropy provides competitive results on certain architectures but lacks the direct decision boundary interpretation that makes logit gap effective. Mean-normalized logit deviation offers incremental improvements over raw values but still underperformed compared to the gap measure. The logit gap’s exceptional performance stems from its unique ability to distill prediction uncertainty into a minimal yet complete representation

that aligns naturally with classification decision boundaries, enabling efficient parameterization while maintaining robust calibration across diverse model types.

5 Conclusion and Limitation

We introduced SMART, a lightweight recalibration method leveraging the logit gap as a principled calibration indicator for precise temp adjustment. By capturing decision boundary uncertainty through this scalar signal, SMART achieves SOTA calibration performance with minimal parameters compared to existing methods. Our SoftECE objective enables stable optimization even with extremely limited val data. Extensive experiments confirm SMART’s robustness across diverse architectures, datasets, and challenging distribution shifts, consistently outperforming TS, PTS, CTS and Spline calibration. Future work could explore integrating SMART with other uncertainty quantification methods to further improve calibration and robustness in safety-critical applications.

Limitation While SMART demonstrates excellent performance across tested scenarios, its effectiveness may vary slightly for extremely specialized domains with highly skewed class distributions. Additionally, though our method requires minimal validation data, performance could degrade in zero-shot scenarios where no domain-specific calibration samples are available.

References

- [1] Chuan Guo, Geoff Pleiss, Yu Sun, and Kilian Q Weinberger. On calibration of modern neural networks. In *Proceedings of the 34th International Conference on Machine Learning (ICML)*, pages 1321–1330. PMLR, 2017.
- [2] Mahdi Pakdaman Naeini, Gregory Cooper, and Milos Hauskrecht. Obtaining well calibrated probabilities using bayesian binning. *Proceedings of the Twenty-Ninth AAAI Conference on Artificial Intelligence*, 2015.
- [3] Bianca Zadrozny and Charles Elkan. Obtaining calibrated probability estimates from decision trees and naive bayesian classifiers. In *Proceedings of the Eighteenth International Conference on Machine Learning*, pages 609–616. Morgan Kaufmann Publishers Inc., 2001.
- [4] Yoni Frenkel, Arseny Potapov, and Sivan Avidar. Network calibration using differentiable classification performance metrics. In *ICASSP 2021-2021 IEEE International Conference on Acoustics, Speech and Signal Processing*, pages 3220–3224. IEEE, 2021.
- [5] Meelis Kull, Miquel Perello Nieto, Markus Kängsepp, Telmo Silva Filho, Hao Song, and Peter Flach. Beyond temperature scaling: Obtaining well-calibrated multi-class probabilities with dirichlet calibration. In *Advances in Neural Information Processing Systems*, pages 12316–12326, 2019.
- [6] Christian Tomani, Daniel Cremers, and Florian Buettner. Parameterized temperature scaling for boosting the expressive power in post-hoc uncertainty calibration. In *Computer Vision – ECCV 2022*, volume 13673 of *Lecture Notes in Computer Science*, pages 555–569. Springer, 2022.
- [7] Aviral Kumar, Sunita Sarawagi, and Ujjwal Jain. Trainable calibration measures for neural networks from kernel mean embeddings. In *International Conference on Machine Learning*, pages 2805–2814. PMLR, 2018.
- [8] Archit Karandikar, Nicholas Cain, Dustin Tran, Balaji Lakshminarayanan, Jonathon Shlens, Michael C Mozer, and Becca Roelofs. Soft calibration objectives for neural networks. *Advances in Neural Information Processing Systems*, 34:29768–29779, 2021.
- [9] Mahdi Pakdaman Naeini, Gregory Cooper, and Milos Hauskrecht. Obtaining well calibrated probabilities using bayesian binning. In *Proceedings of the AAAI Conference on Artificial Intelligence*, volume 29, 2015.
- [10] Kartik Gupta, Amir Rahimi, Thalaiyasingam Ajanthan, Thomas Mensink, Cristian Sminchisescu, and Richard Hartley. Calibration of neural networks using splines. In *International Conference on Learning Representations*, 2021.
- [11] Lu Yang, Kai Zhang, Qing Wang, Sanvesh Zhang, and Caroline Uhler. Beyond global calibration: Group calibration via multiple comparison errors. *arXiv preprint arXiv:2401.15798*, 2024.
- [12] Miao Xiong, Ailin Deng, Pang Wei Koh, Jiaying Wu, Shen Li, Jianqing Xu, and Bryan Hooi. Proximity-informed calibration for deep neural networks. In *Thirty-seventh Conference on Neural Information Processing Systems*, 2023.
- [13] Ursula Hebert-Johnson, Michael Kim, Omer Reingold, and Guy Rothblum. Multicalibration: Calibration for the (computationally-identifiable) masses. *Proceedings of the 35th International Conference on Machine Learning*, 2018.
- [14] Glenn W Brier. Verification of forecasts expressed in terms of probability. *Monthly Weather Review*, 78(1):1–3, 1950.
- [15] Christian Szegedy, Vincent Vanhoucke, Sergey Ioffe, Jon Shlens, and Zbigniew Wojna. Rethinking the inception architecture for computer vision. In *Proceedings of the IEEE Conference on Computer Vision and Pattern Recognition*, pages 2818–2826, 2016.
- [16] Jishnu Mukhoti, Viveka Kulharia, Amartya Sanyal, Stuart Golodetz, Philip Torr, and Puneet Dokania. Calibrating deep neural networks using focal loss. In *Advances in Neural Information Processing Systems*, pages 15744–15755, 2020.

- [17] Linxi Tao, Mingming Dong, and Chang Xu. Dual focal loss for calibration. In *Proceedings of the 40th International Conference on Machine Learning (ICML)*. PMLR, 2023.
- [18] Balaji Lakshminarayanan, Alexander Pritzel, and Charles Blundell. Simple and scalable predictive uncertainty estimation using deep ensembles. In *Advances in Neural Information Processing Systems*, pages 6402–6413, 2017.
- [19] Yarin Gal and Zoubin Ghahramani. Dropout as a bayesian approximation: Representing model uncertainty in deep learning. In *International Conference on Machine Learning*, pages 1050–1059, 2016.
- [20] Marcel Conde, Danny Niebling, Nicolas Schilling, and Bernhard Sick. Approaching the limit of accuracy: Residual uncertainty via test-time data augmentation. In *2023 IEEE International Conference on Data Mining*, pages 933–938. IEEE, 2023.
- [21] Jize Zhang, Bhavya Kailkhura, and T. Yong-Jin Han. Mix-n-match: Ensemble and compositional methods for uncertainty calibration in deep learning. In *International Conference on Machine Learning*, pages 11117–11128. PMLR, 2020.
- [22] Amir Rahimi, Amirreza Shaban, Ching-An Cheng, Byron Boots, and Richard Hartley. Intra order-preserving functions for calibration of multi-class neural networks. In *Advances in Neural Information Processing Systems*, pages 15829–15839, 2020.
- [23] Yuchi Liu, Lei Wang, Yuli Zou, James Zou, and Liang Zheng. Optimizing calibration by gaining aware of prediction correctness. *arXiv preprint arXiv:2404.13016*, 2024.
- [24] Alex Krizhevsky and Geoffrey Hinton. Learning multiple layers of features from tiny images. Technical report, University of Toronto, 2009. Technical Report.
- [25] Jia Deng, Wei Dong, Richard Socher, Li-Jia Li, Kai Li, and Li Fei-Fei. ImageNet: A large-scale hierarchical image database. In *Proceedings of the IEEE Conference on Computer Vision and Pattern Recognition (CVPR)*, pages 248–255. IEEE, 2009.
- [26] Dan Hendrycks and Thomas G. Dietterich. Benchmarking neural network robustness to common corruptions and perturbations. In *International Conference on Learning Representations (ICLR) Workshops*, 2019. ArXiv preprint arXiv:1903.12261.
- [27] Ziwei Liu, Yifan Wang, Yue Song, Changhu Dong, Jie Huang, Li Huang, and Silvio Savarese. Large-scale long-tailed recognition in an open world. In *Proceedings of the IEEE/CVF Conference on Computer Vision and Pattern Recognition (CVPR)*, pages 2533–2542. IEEE, 2019.
- [28] Peng Wang, Yuning Xiong, Ci Chang, Zhanyu Liu, Tian Huang, and Yi-Zhe Fu. Learning to recognize sketches: The ImageNet-Sketch benchmark. In *Proceedings of the IEEE/CVF International Conference on Computer Vision Workshops (ICCVW)*, pages 6486–6495. IEEE, 2019.
- [29] Kaiming He, Xiangyu Zhang, Shaoqing Ren, and Jian Sun. Deep residual learning for image recognition. In *Proceedings of the IEEE/CVF Conference on Computer Vision and Pattern Recognition*, pages 770–778, 2016.
- [30] Sergey Zagoruyko and Nikos Komodakis. Wide residual networks. In *Proceedings of the British Machine Vision Conference*, 2016.
- [31] Gao Huang, Zhuang Liu, Laurens Van Der Maaten, and Kilian Q Weinberger. Densely connected convolutional networks. In *Proceedings of the IEEE/CVF Conference on Computer Vision and Pattern Recognition*, pages 4700–4708, 2017.
- [32] Jishnu Mukhoti, Lukas Kirsch, and Yarin Gal. Estimating uncertainty in deep learning with explicit density models. *arXiv preprint arXiv:2010.05710*, 2020.
- [33] Adam Paszke, Sam Gross, Francisco Massa, Adam Lerer, James Bradbury, Gregory Chanan, Trevor Killeen, Zeming Lin, Natalia Gimelshein, Luca Antiga, et al. Pytorch: An imperative style, high-performance deep learning library. *Advances in Neural Information Processing Systems*, 32:8024–8035, 2019.

- [34] Ze Liu, Yutong Lin, Yutong Cao, Han Hu, Yixuan Wei, Zheng Zhang, Stephen Lin, and Baining Guo. Swin transformer: Hierarchical vision transformer using shifted windows. In *Proceedings of the IEEE/CVF International Conference on Computer Vision*, pages 10012–10022, 2021.
- [35] Alexey Dosovitskiy, Lucas Beyer, Alexander Kolesnikov, Dirk Weissenborn, Xiaohua Zhai, Thomas Unterthiner, Mostafa Dehghani, Matthias Minderer, Georg Heigold, Sylvain Gelly, et al. An image is worth 16x16 words: Transformers for image recognition at scale. In *Proceedings of the International Conference on Learning Representations*, 2021.
- [36] Lior Frenkel and Jacob Goldberger. Network calibration by class-based temperature scaling. In *Proceedings of the 29th European Signal Processing Conference (EUSIPCO)*, pages 1486–1490. IEEE, 2021.
- [37] Ananya Kumar, Percy S. Liang, and Tengyu Ma. Verified uncertainty calibration. In *Advances in Neural Information Processing Systems*, volume 32, pages 3792–3803. Curran Associates, Inc., 2019.

A Theoretical Proofs

Proof of Proposition 3.1 and 3.2. We use $M = \arg \max_j z_j$ and $\mu = \arg \max_{j \neq \max} z_j$ to denote the indices of the first and the second largest values, Eq. (11) is equivalent to

$$\frac{1}{1 + \sum_{j \neq M} e^{(z_j - z_M)/T}} = \hat{p} \quad (12)$$

$$\Leftrightarrow \sum_{j \neq M} e^{(z_j - z_M)/T} = \frac{1}{\hat{p}} - 1. \quad (13)$$

Let $S = \frac{1}{\hat{p}} - 1 \in (0, K - 1)$, we have

$$\sum_{j \neq M} e^{(z_j - z_M)/T} = S. \quad (14)$$

Consider a special case where $z_j - z_M = -\delta$ for all $j \neq M$, then T can be solved explicitly as a function of δ , *i.e.*,

$$(K - 1)e^{-\delta/T} = S \quad (15)$$

$$\Leftrightarrow T = -\frac{\delta}{\log(\frac{S}{K-1})} \in (0, +\infty). \quad (16)$$

Therefore, with arbitrary logits from the model output, even the maximum logit is given, the value choice of T is still undetermined. Such unboundedness is also empirically observed for some other scaling indicators. Nevertheless, the proposed indicator of logit gap effectively bounds the choice of temperature values. Considering the following inequality:

$$\forall j \notin \{M, \mu\}, \quad -\infty < z_j - z_M \leq -g. \quad (17)$$

We substitute Eq. (17) into Eq. (11) and obtain

$$e^{-g/T} < \sum_{j \neq M} e^{(z_j - z_M)/T} = S \leq (K - 1)e^{-g/T}, \quad (18)$$

which bounds T as

$$-\frac{g}{\log(S)} < T \leq -\frac{g}{\log(S/(n - 1))}. \quad (19)$$

B Logit Gap Perspective on Calibration: Revealing Hidden Patterns

Traditional calibration analysis evaluates models from an overall perspective, potentially masking important sample-specific miscalibration patterns. By examining calibration behavior across the continuous spectrum of logit gap values, we uncover fundamental insights about how neural networks distribute confidence and why existing calibration methods often fall short. This analysis provides crucial validation for our theoretical framework established in Section 3.4 and design choices made in Section 3.2.

Revealing Hidden Calibration Heterogeneity Through Logit Gap Groupings Our reliability diagram analysis unveils a crucial insight that traditional overall calibration metrics obscure: models exhibit fundamentally different calibration behaviors across logit gap groups. This heterogeneity validates our theoretical framework from Section 3.4 while revealing why sample-specific calibration approaches are essential for achieving truly reliable uncertainty estimates.

Figure 5 demonstrates this heterogeneity across different scenarios. For ImageNet with ViT-B/16, while overall calibration appears near-perfect (Figure 5a), decomposing by logit gap reveals distinct patterns: low gap samples achieve almost perfect but slightly under-confident calibration (Figure 5c), while high gap samples suffer from systematic miscalibration (Figure 5b). This pattern persists even under different overall calibration conditions, as shown in CIFAR-100 with ResNet-50 (Figures 5d and 5e), indicating that logit gap-based groupings reveal fundamental calibration characteristics that transcend dataset-specific or architecture-specific behaviors.

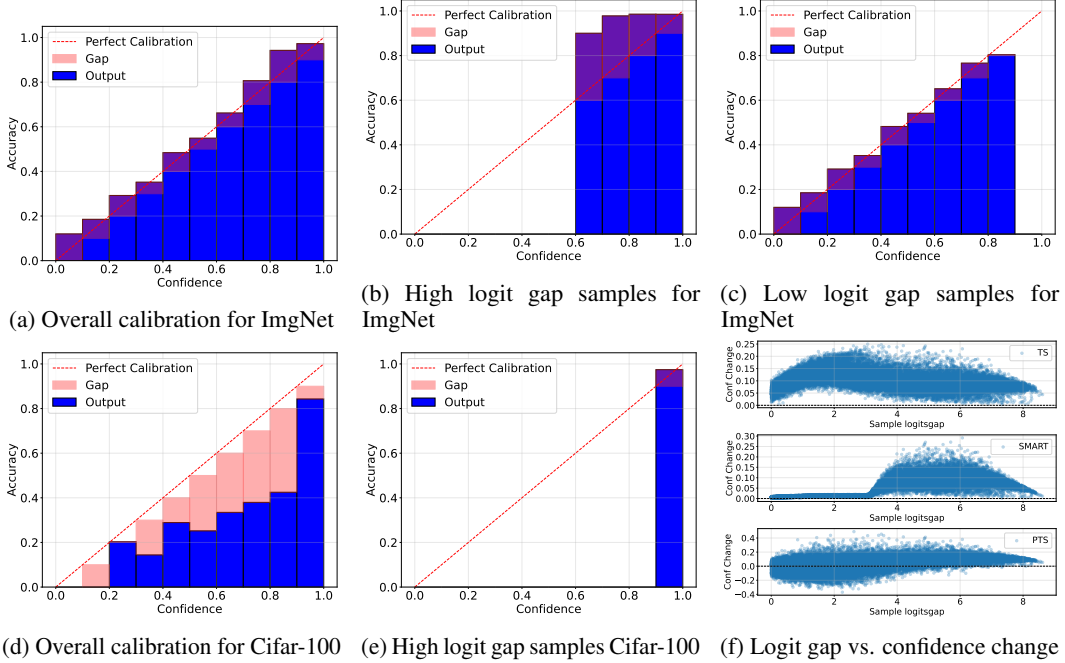


Figure 5: Logit gap reveals hidden calibration patterns across the confidence spectrum. Top row: ImageNet ViT-B/16 shows almost perfect but slightly under-confident overall calibration (a) but reveals systematic under-confidence in high logit gap samples (b) and almost well-calibrated but slightly under-confident low logit gap samples (c). Bottom row: CIFAR-100 ResNet-50 demonstrates that even with overall over-confidence (d), high logit gap samples remain under-confident (e). Panel (f) shows how different methods adjust confidence across logit gap values, with SMART providing targeted adjustments while TS and PTS show suboptimal patterns.

The Under-Confidence Paradox in High Logit Gap Samples Perhaps the most counterintuitive finding emerges from examining high logit gap samples across our reliability diagrams. Despite representing "easy" classifications with substantial margins between top predictions, these samples consistently exhibit under-confidence rather than the expected over-confidence. In Figure 5b, high gap samples from ImageNet ViT-B/16 show systematic under-confidence, with predicted confidence consistently lower than empirical accuracy. This pattern holds even when overall model behavior differs dramatically, as demonstrated in Figure 5e where CIFAR-100 ResNet-50 maintains under-confidence in high gap samples despite overall over-confidence.

This paradox fundamentally challenges conventional intuitions about neural network confidence and validates our theoretical analysis from Section 3.4. High logit gap samples, despite being far from decision boundaries, require confidence enhancement rather than reduction. This phenomenon suggests that modern neural networks, when trained with standard cross-entropy objectives, develop conservative confidence estimates for samples with clear classification margins. The consistency of this pattern across different architectures and datasets indicates that this represents a fundamental characteristic of neural network training dynamics rather than an artifact of specific experimental conditions.

Method-Specific Failures from the Logit Gap Perspective The confidence adjustment patterns revealed in Figure 5f expose fundamental limitations in existing calibration approaches when viewed through the logit gap lens. Temperature Scaling’s uniform adjustment completely ignores the heterogeneous calibration needs we identified, applying identical modifications regardless of sample characteristics. This uniform approach proves particularly problematic because it fails to provide the targeted adjustments different gap groups require.

More critically, PTS demonstrates the exact problems we highlighted in Section 3.2 regarding high-dimensional parameterization introducing noise. The method makes substantial, often counterproductive adjustments to low logit gap samples that, in cases like ImageNet ViT-B/16, already achieve good calibration and require minimal intervention. This unnecessary manipulation ex-

emphasizes how "the increased dimensionality introduces substantial noise for precise temperature parameterization," leading to degraded performance where careful preservation of existing calibration would be more appropriate.

In contrast, SMART’s learned adjustment pattern directly validates our design principles. For ImageNet ViT-B/16, SMART provides minimal adjustments to low gap samples that are already well-calibrated, while delivering targeted confidence increases to high gap samples suffering from under-confidence. This adaptive behavior emerges naturally from our lightweight scalar-to-scalar mapping, demonstrating how principled architectural choices translate into appropriate calibration strategies without requiring explicit programming of these patterns.

Theoretical Validation and Design Implications These empirical findings provide compelling validation for our theoretical framework established in Propositions 3.1 and 3.2. The systematic under-confidence in high logit gap samples directly supports our argument that temperature values should be bounded by logit gaps rather than determined by global statistics or high-dimensional features. The fact that SMART automatically learns to provide confidence enhancement for high gap samples while preserving the calibration of well-adjusted low gap samples demonstrates the practical effectiveness of our theoretical bounds.

C The proposed SMART framework

This section presents the detailed algorithmic implementation of SMART, providing a step-by-step procedure for applying logit gap-based temperature scaling with soft-binned ECE optimization.

Algorithm 1 The proposed SMART framework

- 1: **Input:** Validation logits and labels $\{\mathbf{z}_i, y_i\}_{i=1}^N$, temperature parameterization network $h_\phi(\cdot)$.
 - 2: Compute logit gaps $g_i = \mathbf{z}_{i,\max} - \mathbf{z}_{i,2\text{nd}}$ for each sample i .
 - 3: Normalize: $\hat{g}_i = \frac{g_i - \mu_g}{\sigma_g}$
 - 4: **for** each epoch **do**
 - 5: Compute sample-wise temperature $T = h_\phi(\hat{g}_i)$ for each sample i .
 - 6: Compute calibrated logits $\hat{\mathbf{z}}_i = \mathbf{z}_i / T$ for each sample i .
 - 7: Compute loss $\mathcal{L}_i = \text{SoftECE}(\hat{\mathbf{z}}_i, y_i)$ for each sample i .
 - 8: Update parameters ϕ using gradient descent from the overall loss $\mathcal{L}_{\text{calib}} = \sum_{i=1}^N \mathcal{L}_i$
 - 9: **end for**
-

D Calibration Performance on Other Metrics

D.1 Accuracy Performance

Accuracy Preservation Analysis Table 6 confirms that SMART achieves superior calibration while perfectly preserving classification accuracy—a fundamental advantage of post-hoc methods. Unlike CTS, which suffers accuracy drops up to 1.48 percentage points due to class-specific boundary alterations, or Spline’s variable impacts on transformers, SMART’s design ensures zero accuracy loss. By operating exclusively on the logit gap rather than full logit vectors, SMART focuses solely on confidence scaling without disturbing the relative ordering that determines predictions. This preservation holds even under severe distribution shifts like ImageNet-C and ImageNet-Sketch, where SMART simultaneously maintains base model accuracy while dramatically improving calibration. This dual guarantee makes SMART uniquely suitable for safety-critical applications requiring both correct predictions and reliable uncertainty estimates.

D.2 AdaECE Performance

This section provides an in-depth analysis of calibration performance using AdaECE across different datasets and model architectures, complementing the results presented in Section 4.2. Adaptive-ECE is a measure of calibration performance that addresses the bias of equal-width binning scheme of ECE. It adapts the bin-size to the number of samples and ensures that each bin is evenly distributed with samples. The formula for Adaptive-ECE is as follows:

$$\text{Adaptive-ECE} = \sum_{i=1}^{\mathbb{B}} \frac{|B_i|}{N} |I_i - C_i| \text{ s.t. } \forall i, j \cdot |B_i| = |B_j| \quad (20)$$

Table 6: **Comparison of Classification Accuracy (%) Across Calibration Methods (Seed 1–5 Averaged).**

Dataset	Model	Vanilla	TS	PTS	CTS	Spline	SMART
CIFAR-10	ResNet-50	95.05%	95.05%	95.05%	94.88%	95.05%	95.05%
	Wide-ResNet	96.13%	96.13%	96.13%	96.09%	96.13%	96.13%
CIFAR-100	ResNet-50	76.69%	76.69%	76.69%	76.38%	76.69%	76.69%
	Wide-ResNet	79.29%	79.29%	79.29%	79.28%	79.29%	79.29%
ImageNet-1K	ResNet-50	76.16%	76.16%	76.16%	75.32%	76.17%	76.16%
	DenseNet-121	74.44%	74.44%	74.44%	73.71%	74.43%	74.44%
	Wide-ResNet	78.46%	78.46%	78.46%	77.70%	78.46%	78.46%
	Swin-B	83.17%	83.17%	83.17%	82.80%	83.17%	83.17%
	ViT-B-16	81.12%	81.12%	81.12%	79.64%	80.86%	81.12%
	ViT-B-32	75.95%	75.95%	75.95%	75.14%	75.94%	75.95%
ImageNet-C	ResNet-50	19.16%	19.16%	19.16%	19.34%	19.16%	19.16%
	DenseNet-121	21.25%	21.25%	21.25%	21.36%	21.25%	21.25%
	Swin-B	40.83%	40.83%	40.83%	41.22%	40.83%	40.83%
	ViT-B-16	41.07%	41.07%	41.07%	41.28%	41.07%	41.07%
	ViT-B-32	37.82%	37.82%	24.56%	37.96%	37.85%	37.82%
ImageNet-LT	ResNet-50	76.04%	76.04%	76.04%	75.43%	76.04%	76.04%
	DenseNet-121	74.34%	74.34%	74.34%	73.88%	74.40%	74.34%
	Wide-ResNet	78.39%	78.39%	78.39%	77.67%	78.40%	78.39%
	Swin-B	82.95%	82.95%	82.95%	82.55%	82.94%	82.95%
	ViT-B-16	80.95%	80.95%	80.95%	80.58%	81.00%	80.95%
	ViT-B-32	75.89%	75.89%	75.89%	75.14%	75.92%	75.89%
ImageNet-S	ResNet-50	24.09%	24.09%	24.09%	23.88%	24.09%	24.09%
	DenseNet-121	24.30%	24.30%	24.30%	23.87%	24.30%	24.30%
	Swin-B	31.54%	31.54%	31.54%	31.65%	31.55%	31.54%
	ViT-B-16	29.37%	29.37%	29.37%	29.51%	29.39%	29.37%
	ViT-B-32	27.77%	27.77%	27.77%	27.76%	27.75%	27.77%

AdaECE offers a more rigorous assessment of calibration quality than standard ECE by adapting bin boundaries to ensure uniform sample distribution, preventing calibration errors from being masked in sparsely populated confidence regions. Table 7 presents comprehensive AdaECE results across all evaluated datasets and architectures. SMART consistently outperforms competing methods under this metric, achieving the lowest AdaECE on 24 of 26 dataset-architecture combinations.

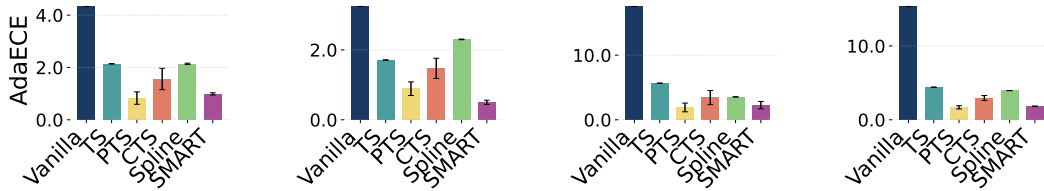


Figure 6: **AdaECE comparison on CIFAR datasets.** SMART consistently achieves superior calibration on both CIFAR-10 and CIFAR-100 across multiple architectures. From left to right are Cifar10 ResNet-50/Wide-ResNet, Cifar100 ResNet-50/Wide-ResNet.

CIFAR Performance Analysis. SMART demonstrates exceptional calibration on CIFAR datasets in Figure 6, achieving the lowest AdaECE with notably stable variance compared to competitors. The key insight emerges when comparing CIFAR-10 to CIFAR-100: while global methods like TS suffer dramatic degradation as class count increases, SMART maintains robust performance. PTS shows competitive results but with substantially higher variance, indicating reliability issues. Spline struggles particularly with CIFAR-100’s complex confidence landscape, revealing how non-parametric methods become less effective as classification complexity increases.

Large-Scale Classification on ImageNet. In Figure 7, The ImageNet results reveal a crucial architectural insight: SMART maintains consistent performance across both CNN and transformer designs, while traditional methods like TS and CTS show pronounced degradation on transformers. This architectural robustness highlights SMART’s ability to capture fundamental uncertainty signals through the logit gap regardless of model inductive biases. PTS exhibits extreme variance, confirming

Table 7: **Comparison of AdaECE Calibration Methods Using AdaECE(\downarrow , %, 15bins) Across Various Datasets and Models (Seed 1–5 Averaged).**

Dataset	Model	Vanilla	TS	PTS	CTS	Spline	SMART
CIFAR-10	ResNet-50	4.33 \pm 0.0%	2.14 \pm 0.0%	0.83 \pm 28.6%	1.56 \pm 26.2%	2.14 \pm 1.1%	0.99 \pm 4.3%
	Wide-ResNet	3.24 \pm 0.0%	1.71 \pm 0.0%	0.89 \pm 21.9%	1.47 \pm 19.7%	2.30 \pm 0.4%	0.50 \pm 12.2%
CIFAR-100	ResNet-50	17.53 \pm 0.0%	5.66 \pm 0.0%	1.91 \pm 35.3%	3.43 \pm 32.0%	3.55 \pm 0.0%	2.27 \pm 25.2%
	Wide-ResNet	15.34 \pm 0.0%	4.41 \pm 0.0%	1.69 \pm 13.0%	2.95 \pm 11.6%	3.95 \pm 0.1%	1.83 \pm 2.1%
ImageNet-1K	ResNet-50	3.68 \pm 1.3%	2.13 \pm 0.5%	0.92 \pm 44.1%	2.21 \pm 39.8%	0.81 \pm 28.7%	0.79 \pm 8.7%
	DenseNet-121	2.52 \pm 1.4%	1.74 \pm 1.8%	1.05 \pm 41.3%	1.78 \pm 38.0%	0.77 \pm 28.0%	0.65 \pm 10.2%
	Wide-ResNet	5.31 \pm 0.3%	2.87 \pm 2.8%	1.04 \pm 20.6%	3.24 \pm 18.0%	0.83 \pm 36.3%	0.87 \pm 14.3%
	Swin-B	4.86 \pm 0.6%	4.50 \pm 1.0%	1.05 \pm 4.6%	1.59 \pm 5.1%	1.04 \pm 5.3%	0.74 \pm 12.2%
	ViT-B-16	5.57 \pm 1.2%	4.10 \pm 2.3%	1.09 \pm 29.7%	4.85 \pm 27.4%	1.07 \pm 29.2%	0.79 \pm 15.4%
	ViT-B-32	6.41 \pm 0.4%	3.92 \pm 1.7%	1.27 \pm 71.9%	1.90 \pm 66.4%	0.96 \pm 15.3%	0.78 \pm 3.6%
ImageNet-C	ResNet-50	13.84 \pm 0.2%	2.02 \pm 1.7%	1.06 \pm 0.7%	1.76 \pm 0.6%	5.49 \pm 2.8%	0.74 \pm 8.0%
	DenseNet-121	12.57 \pm 0.1%	1.64 \pm 0.7%	1.17 \pm 9.9%	1.48 \pm 8.2%	2.57 \pm 7.9%	0.70 \pm 3.6%
	Swin-B	11.98 \pm 0.1%	5.83 \pm 1.0%	1.58 \pm 0.0%	3.07 \pm 0.2%	5.13 \pm 2.3%	1.31 \pm 2.9%
	ViT-B-16	8.24 \pm 0.3%	5.25 \pm 0.9%	1.27 \pm 5.9%	2.77 \pm 5.3%	2.57 \pm 7.9%	1.09 \pm 4.0%
	ViT-B-32	7.66 \pm 0.2%	5.11 \pm 0.0%	1.07 \pm 4.3%	2.97 \pm 3.7%	1.45 \pm 16.8%	1.01 \pm 4.2%
ImageNet-LT	ResNet-50	3.54 \pm 0.9%	2.02 \pm 1.2%	0.92 \pm 35.5%	2.17 \pm 33.0%	0.71 \pm 20.7%	0.67 \pm 3.3%
	DenseNet-121	2.37 \pm 3.4%	1.74 \pm 2.1%	1.17 \pm 23.6%	1.86 \pm 21.3%	0.73 \pm 26.4%	0.76 \pm 0.7%
	Wide-ResNet	5.22 \pm 0.4%	2.98 \pm 0.9%	1.22 \pm 62.4%	2.83 \pm 58.1%	0.79 \pm 18.1%	0.98 \pm 4.4%
	Swin-B	4.69 \pm 0.6%	4.48 \pm 1.2%	1.43 \pm 19.1%	1.23 \pm 18.0%	0.95 \pm 6.7%	0.74 \pm 31.3%
	ViT-B-16	5.57 \pm 0.8%	4.18 \pm 2.9%	1.13 \pm 43.4%	1.06 \pm 40.1%	0.95 \pm 12.9%	0.85 \pm 15.1%
	ViT-B-32	6.26 \pm 0.6%	3.97 \pm 1.6%	1.30 \pm 31.1%	2.04 \pm 28.2%	0.86 \pm 26.5%	0.84 \pm 10.1%
ImageNet-S	ResNet-50	22.31 \pm 0.3%	2.01 \pm 2.9%	1.64 \pm 16.4%	1.51 \pm 14.7%	9.51 \pm 2.4%	0.90 \pm 15.8%
	DenseNet-121	20.15 \pm 0.5%	1.67 \pm 17.0%	1.93 \pm 9.6%	1.16 \pm 8.3%	8.7 \pm 1.92%	0.76 \pm 32.3%
	Swin-B	24.62 \pm 0.0%	6.40 \pm 0.5%	1.53 \pm 12.2%	3.57 \pm 11.1%	9.06 \pm 4.2%	1.53 \pm 3.8%
	ViT-B-16	16.57 \pm 0.2%	5.62 \pm 0.7%	1.33 \pm 8.7%	2.98 \pm 7.3%	8.66 \pm 1.9%	1.08 \pm 4.3%
	ViT-B-32	14.19 \pm 0.3%	4.98 \pm 2.9%	1.66 \pm 16.0%	3.23 \pm 14.1%	5.64 \pm 3.3%	1.07 \pm 19.9%

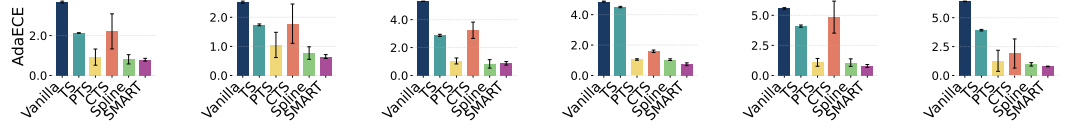


Figure 7: **AdaECE(\downarrow , %, 15bins) comparison on ImageNet-1K.** SMART delivers consistent calibration across diverse architectures, from CNNs to vision transformers. From left to right are ResNet-50, DenseNet-121, Wide-ResNet, Swin-B, ViT-B-16, ViT-B-32.

that high-dimensional parameterizations struggle with reliability when learning complex temperature mappings, particularly on large-scale datasets.

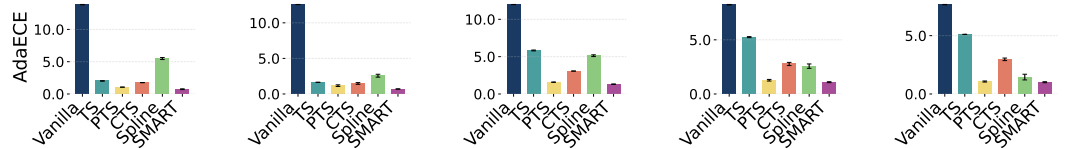


Figure 8: **AdaECE(\downarrow , %, 15bins) comparison on ImageNet-C.** SMART maintains exceptional calibration under corruption, while Spline and TS-based methods demonstrate significant degradation. From left to right are ResNet-50, DenseNet-121, Swin-B, ViT-B-16, ViT-B-32.

Robustness to Input Corruption. As shown in Figure 8, SMART’s resilience under corruption provides compelling evidence for the stability of decision boundary information. While Spline performs competitively on clean ImageNet, it deteriorates dramatically under corruption with values 5-7 \times higher than SMART. This collapse reveals a fundamental limitation: non-parametric methods overfit to validation distributions and fail when input characteristics change. SMART’s focus on decision boundary uncertainty via the logit gap remains informative even when input distributions shift substantially.

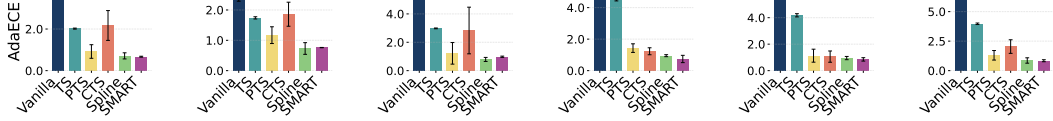


Figure 9: **AdaECE(\downarrow , %, 15bins) comparison on ImageNet-LT.** SMART maintains strong calibration under long-tailed class distributions, particularly on CNN architectures. From left to right are ResNet-50, DenseNet-121, Wide-ResNet, Swin-B, ViT-B-16, ViT-B-32.

Long-Tailed Distribution Calibration. As shown in Figure 9, The ImageNet-LT results reveal that class imbalance presents a fundamentally different calibration challenge than input corruption. Interestingly, Spline performs competitively here, suggesting non-parametric methods can handle statistical imbalances better than distributional shifts. However, CTS underperforms despite being explicitly designed for per-class variations, demonstrating that simply applying different temperatures per class is insufficient for complex imbalanced scenarios.

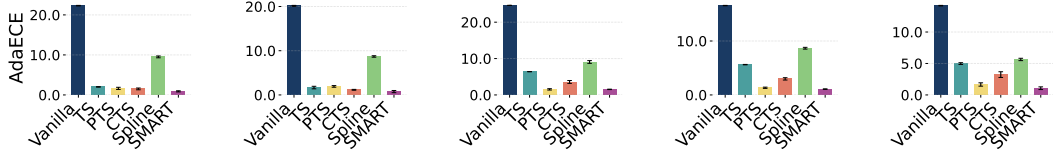


Figure 10: **AdaECE(\downarrow , %, 15bins) comparison on ImageNet-Sketch.** SMART maintains exceptional calibration under extreme domain shift, while Spline struggles significantly. From left to right are ResNet-50, DenseNet-121, Swin-B, ViT-B-16, ViT-B-32.

Extreme Domain Shift Calibration. The sketch-based domain shift represents the most challenging calibration scenario in Figure 10, where SMART demonstrates its most dramatic advantage. Spline’s collapse here reinforces the brittleness of non-parametric methods under distribution shifts, while SMART’s consistent performance across all architectures provides strong evidence that logit gap information captures robust uncertainty signals that transcend specific input characteristics or domains.

E Comparison Of Various Training-Time Calibration Methods On Other Metrics

This section presents a comprehensive evaluation of SMART when combined with various training-time calibration methods across multiple metrics, extending the ECE analysis provided in Section 4.3. We examine SMART’s performance using AdaECE, Classwise ECE (CECE), Negative Log-Likelihood (NLL), and classification accuracy.

E.1 Accuracy Preservation

Dataset	Model	Cross-Entropy		Brier Loss		MMCE		LS-0.05		FLSD-53		FL-3	
		base	ours	base	ours	base	ours	base	ours	base	ours	base	ours
CIFAR10	ResNet-50	95.1	95.1	95.0	95.0	95.0	95.0	94.7	94.7	95.0	95.0	94.8	94.8
	ResNet-110	95.1	95.1	94.5	94.5	94.6	94.6	94.5	94.5	94.6	94.6	94.9	94.9
	DenseNet-121	95.0	95.0	94.9	94.9	94.6	94.6	94.9	94.9	94.6	94.6	94.7	94.7
	Wide-ResNet	96.1	96.1	95.9	95.9	96.1	96.1	95.8	95.8	96.0	96.0	95.9	95.9
CIFAR100	ResNet-50	76.7	76.7	76.6	76.6	76.8	76.8	76.6	76.6	76.8	76.8	77.3	77.3
	ResNet-110	77.3	77.3	74.9	74.9	76.9	76.9	76.6	76.6	77.5	77.5	77.1	77.1
	DenseNet-121	75.5	75.5	76.3	76.3	76.0	76.0	75.9	75.9	77.3	77.3	76.8	76.8
	Wide-ResNet	79.3	79.3	79.4	79.4	79.3	79.3	78.8	78.8	79.9	79.9	80.3	80.3

Table 8: **Comparison of Train-time Calibration Methods Using Accuracy(\uparrow , %) Across Various Datasets and Models.** Results demonstrate that SMART preserves the original model accuracy across all training methods. Results are from the best run of 5 seeds.

Accuracy Analysis As shown in Table 8, SMART consistently preserves the classification accuracy of all base models across all training-time calibration methods. This is a critical property of post-hoc calibration methods, as improving confidence estimates should not come at the cost of predictive performance. The perfect accuracy preservation is by design, as SMART’s temperature scaling mechanism operates solely on the scaling of logits without altering their relative ordering, thus maintaining the same class predictions. This contrasts with some training-time methods that may involve trade-offs between accuracy and calibration quality during the model optimization process. The preservation of accuracy across diverse architectures and datasets further validates SMART’s practical utility as a calibration method that can be safely applied in real-world scenarios where maintaining predictive performance is essential.

E.2 AdaECE Performance

Dataset	Model	Cross-Entropy		Brier Loss		MMCE		LS-0.05		FLSD-53		FL-3	
		base	ours	base	ours	base	ours	base	ours	base	ours	base	ours
CIFAR10	ResNet-50	4.33	0.80	1.74	1.01	4.55	0.67	3.88	2.18	1.56	0.45	1.95	0.48
	ResNet-110	4.40	1.22	2.61	0.56	5.07	0.93	4.46	3.66	2.07	0.40	1.64	0.52
	DenseNet-121	4.49	0.61	2.01	0.51	5.10	0.96	4.40	2.95	1.38	0.62	1.23	0.83
	Wide-ResNet	3.24	0.44	1.70	0.44	3.29	0.53	4.27	0.97	1.52	0.44	1.84	0.59
CIFAR100	ResNet-50	17.53	1.00	6.54	1.41	15.31	1.08	7.63	1.75	4.40	1.35	5.08	0.95
	ResNet-110	19.06	1.67	7.73	0.93	19.13	1.98	11.07	2.72	8.54	0.93	8.65	1.22
	DenseNet-121	20.99	2.23	5.04	1.02	19.10	1.73	12.83	1.96	3.54	0.93	4.14	0.97
	Wide-ResNet	15.34	1.55	4.28	0.97	13.16	1.12	5.13	2.11	2.77	0.75	2.07	1.15

Table 9: **Comparison of Train-time Calibration Methods Using AdaECE(\downarrow , %, 15bins) Across Various Datasets and Models.** The best-performing method for each dataset-model combination is in bold, and our method (SMART) is highlighted. Results are from the best run of 5 seeds.

AdaECE Analysis The adaptive ECE results in Table 9 provide further validation of SMART’s effectiveness when combined with various training-time calibration methods. AdaECE, which uses adaptive binning to ensure equal sample counts in each bin, offers a more robust calibration measure than standard ECE by eliminating potential biases from uneven confidence distributions. SMART consistently improves AdaECE across all training methods, with particularly dramatic improvements for models trained with Cross-Entropy and MMCE, where we observe reductions of up to $18\times$ ($17.53\% \rightarrow 1.00\%$ for CIFAR-100 ResNet-50).

The most substantial AdaECE improvements occur on CIFAR-100, which has ten times more classes than CIFAR-10 and thus represents a more challenging calibration scenario. This suggests that SMART’s effectiveness scales favorably with task complexity. Even for models already trained with calibration-oriented objectives like Focal Loss or FLSD, SMART provides further substantial improvements, indicating that its logit gap-based temperature adjustment captures complementary information to these training-time approaches. Notably, the combination of SMART with FLSD-53 achieves some of the lowest overall AdaECE values (e.g., 0.40% on CIFAR-10 ResNet-110), suggesting a particularly effective synergy between these methods.

E.3 Classwise ECE Performance

Dataset	Model	Cross-Entropy		Brier Loss		MMCE		LS-0.05		FLSD-53		FL-3	
		base	ours	base	ours	base	ours	base	ours	base	ours	base	ours
CIFAR10	ResNet-50	0.91	0.43	0.46	0.40	0.94	0.51	0.71	0.51	0.42	0.37	0.43	0.38
	ResNet-110	0.92	0.49	0.59	0.45	1.04	0.54	0.66	0.54	0.47	0.41	0.44	0.38
	DenseNet-121	0.92	0.45	0.46	0.41	1.04	0.59	0.60	0.50	0.41	0.38	0.42	0.35
	Wide-ResNet	0.68	0.37	0.44	0.39	0.70	0.38	0.79	0.40	0.41	0.29	0.44	0.34
CIFAR100	ResNet-50	0.38	0.21	0.22	0.20	0.34	0.20	0.23	0.21	0.20	0.20	0.20	0.20
	ResNet-110	0.41	0.20	0.24	0.21	0.42	0.21	0.26	0.20	0.24	0.20	0.24	0.21
	DenseNet-121	0.45	0.23	0.20	0.20	0.42	0.23	0.29	0.21	0.19	0.20	0.20	0.20
	Wide-ResNet	0.34	0.19	0.19	0.19	0.30	0.19	0.21	0.20	0.18	0.18	0.18	0.18

Table 10: **Comparison of Train-time Calibration Methods Using Classwise ECE(\downarrow , %, 15bins) Across Various Datasets and Models.** The best-performing method for each dataset-model combination is in bold, and our method (SMART) is highlighted. Results are from the best run of 5 seeds.

CECE Analysis Classwise ECE (CECE) provides insights into calibration performance at the individual class level rather than aggregated across all classes. The formula for classwise ECE is:

$$\text{Classwise-ECE} = \frac{1}{\mathcal{K}} \sum_{i=1}^B \sum_{j=1}^{\mathcal{K}} \frac{|B_{i,j}|}{N} |I_{i,j} - C_{i,j}| \quad (21)$$

where the calibration error is computed separately for each class j across all bins i , then averaged across all \mathcal{K} classes. This metric is particularly valuable for understanding whether calibration improvements are uniformly distributed across classes or concentrated in specific categories.

Table 10 demonstrates SMART’s ability to improve per-class calibration across almost all training methods and architectures. The improvements are particularly prominent for models trained with Cross-Entropy and MMCE, where CECE values are typically reduced by 50% or more after applying SMART (e.g., from 0.91% to 0.43% for CIFAR-10 ResNet-50). This substantial improvement suggests that SMART’s logit gap-based temperature scaling effectively addresses class-specific miscalibration patterns that may arise during training with these standard objectives.

Interestingly, CECE values are consistently lower on CIFAR-100 compared to CIFAR-10 despite the higher class count, which contrasts with the pattern observed for ECE and AdaECE. This phenomenon occurs because CECE averages calibration errors across classes, and with 100 classes, individual class miscalibrations tend to average out more effectively than with only 10 classes. Additionally, the higher granularity of class divisions in CIFAR-100 may lead to more balanced per-class confidence distributions, making the averaging effect more pronounced.

For models already trained with calibration-oriented losses like FLSD-53 and FL-3, SMART provides more modest improvements in CECE, and in a few cases maintains the same level of performance. This suggests that these training-time methods are already effective at addressing per-class calibration issues through their specialized loss formulations that inherently consider class-wise balance. However, SMART can still provide complementary benefits in most scenarios, particularly for classes that may remain poorly calibrated even after specialized training procedures.

E.4 Negative Log-Likelihood Performance

Dataset	Model	Cross-Entropy		Brier Loss		MMCE		LS-0.05		FLSD-53		FL-3	
		Base	Ours	Base	Ours	Base	Ours	Base	Ours	Base	Ours	Base	Ours
CIFAR-10	ResNet-50	41.2	19.7	18.7	18.4	44.8	21.0	27.7	27.7	17.6	17.1	18.4	17.9
	ResNet-110	47.5	22.5	20.4	19.4	55.7	23.6	29.9	29.4	18.5	17.9	17.8	17.3
	DenseNet-121	42.9	20.8	19.1	18.6	52.1	24.1	28.7	28.7	18.4	18.1	18.0	17.9
	Wide-ResNet	26.8	14.9	15.9	15.4	28.5	15.9	21.7	19.9	14.6	13.7	15.2	14.9
CIFAR-100	ResNet-50	153.7	105.3	99.6	99.5	125.3	100.7	121.0	120.1	88.0	88.4	87.5	88.1
	ResNet-110	179.2	104.0	110.7	110.0	180.6	106.1	133.1	128.8	89.9	88.3	90.9	90.0
	DenseNet-121	205.6	119.1	98.3	98.9	166.6	112.6	142.0	134.3	85.5	86.5	87.1	87.3
	Wide-ResNet	140.1	95.2	84.6	84.9	119.6	94.1	108.1	106.5	76.9	77.4	74.7	75.8

Table 11: **Comparison of Train-time Calibration Methods Using NLL(↓, %) Across Various Datasets and Models.** The best-performing method for each dataset-model combination is in bold, and our method (SMART) is highlighted. Results are from the best run of 5 seeds.

NLL Analysis NLL is a probabilistic metric that measures both calibration quality and discriminative power. Table 11 shows that SMART improves NLL for most models, with the most significant gains observed for Cross-Entropy, MMCE, and LS-0.05 trained models. The improvements are particularly striking for CIFAR-10, where NLL is reduced by up to 60% after applying SMART (e.g., 41.22 → 19.70 for ResNet-50 with Cross-Entropy).

However, a different pattern emerges for models trained with specialized losses like FLSD-53 and FL-3 on CIFAR-100, where SMART sometimes leads to slight increases in NLL despite improvements in calibration metrics like ECE and AdaECE. This suggests that these specialized training losses optimize directly for NLL-like objectives, creating a scenario where SMART’s temperature scaling might slightly disturb the carefully optimized probability distributions. Nevertheless, the overall trend across metrics indicates that SMART maintains or improves model performance in the vast majority of cases.

F Calibration Performance Under Specific Corruption Types

To provide deeper insights into SMART’s robustness across different corruption scenarios, we examine the calibration error reduction achieved by various methods on individual corruption types in ImageNet-C. We analyze performance across two architectures (ResNet-50 and ViT-B/16) and two metrics (ECE and AdaECE), providing a comprehensive view of how different calibration approaches respond to specific distribution shifts. This granular analysis helps understand which corruption types pose the greatest calibration challenges and how architectural differences influence calibration robustness.

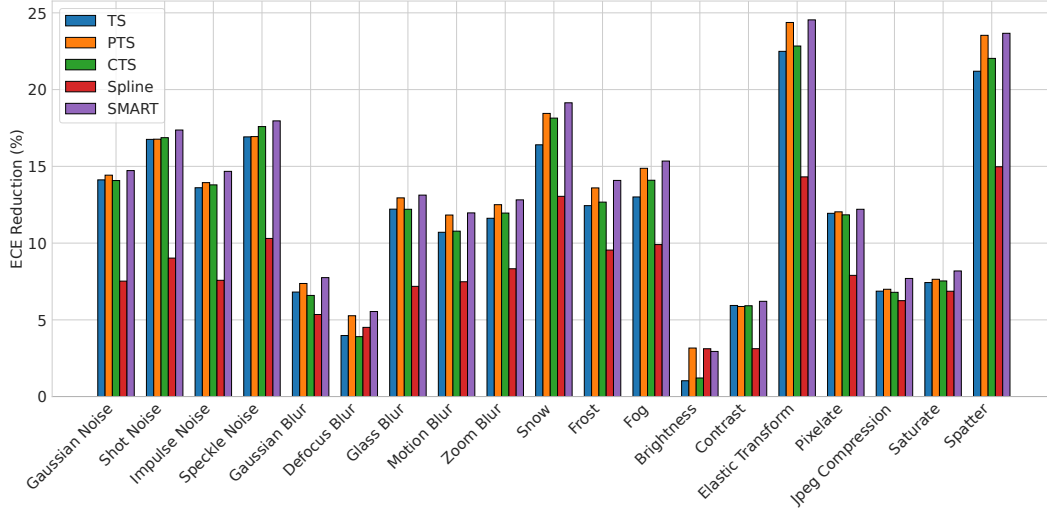


Figure 11: ECE reduction(↑, %, 15bins) across corruption types for ResNet-50. SMART consistently achieves superior calibration improvements across diverse corruption scenarios, demonstrating exceptional robustness to distribution shifts.

ResNet-50 ECE Analysis The corruption-specific analysis reveals that SMART demonstrates remarkable consistency, achieving the highest ECE reduction across most corruption categories with improvements often exceeding 20%. The inclusion of Spline calibration exposes a critical limitation of non-parametric methods: extreme brittleness under distribution shifts. While Spline achieves competitive results on certain corruptions like Snow, it completely fails on others such as Brightness and Contrast, highlighting how non-parametric approaches overfit to validation characteristics and break down when faced with novel corruptions.

This contrasts sharply with SMART’s robust performance across all corruption types. The key insight is that SMART’s logit gap indicator captures decision boundary information that remains meaningful regardless of input degradation type—whether geometric distortions, noise, or digital artifacts. Temperature Scaling and other global methods show predictable limitations on uniform corruptions, while parametric methods like PTS exhibit moderate consistency but still significant variability. SMART’s sample-specific adaptation based on decision boundary information provides the most reliable calibration improvements, making it uniquely suitable for real-world scenarios where corruption characteristics are unpredictable.

ResNet-50 AdaECE Analysis The AdaECE results closely mirror the ECE patterns, confirming that SMART’s calibration improvements are fundamental rather than evaluation artifacts. SMART achieves the highest reduction rates across most corruptions, with particularly strong performance on geometric distortions approaching 25% improvement. Spline’s brittleness persists under adaptive binning—performing reasonably on weather corruptions but failing on uniform transforms, confirming that its limitations stem from overfitting rather than evaluation methodology. The near-identical performance rankings across both metrics demonstrate that SMART’s logit gap approach captures robust calibration signals regardless of how calibration quality is measured.

ViT-B/16 ECE Analysis The transformer results reveal striking architectural differences in calibration behavior under corruption. Most notably, Temperature Scaling frequently worsens calibration,

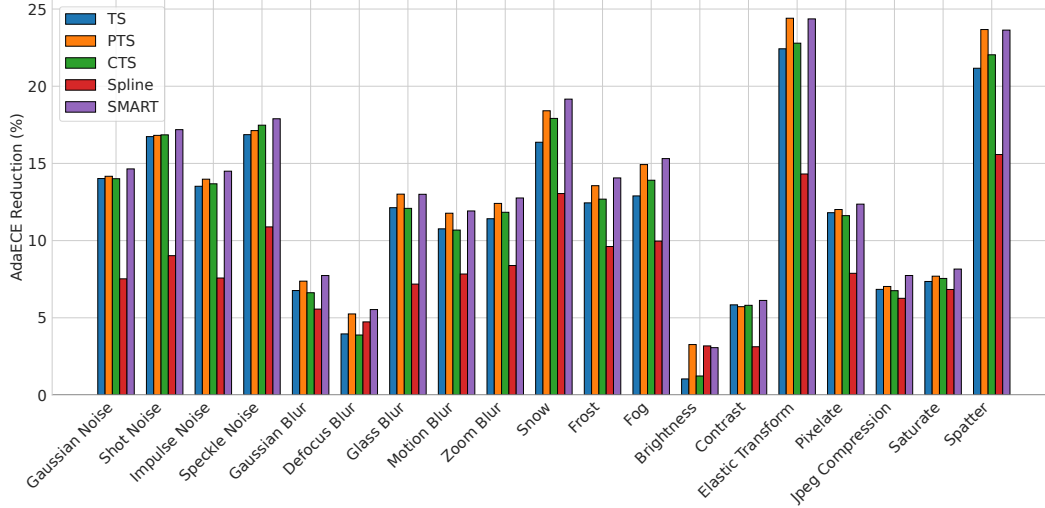


Figure 12: **AdaECE reduction(↑, %, 15bins) across corruption types for ResNet-50.** SMART maintains consistent superiority across corruption types under adaptive binning, confirming robust calibration improvements independent of evaluation methodology.

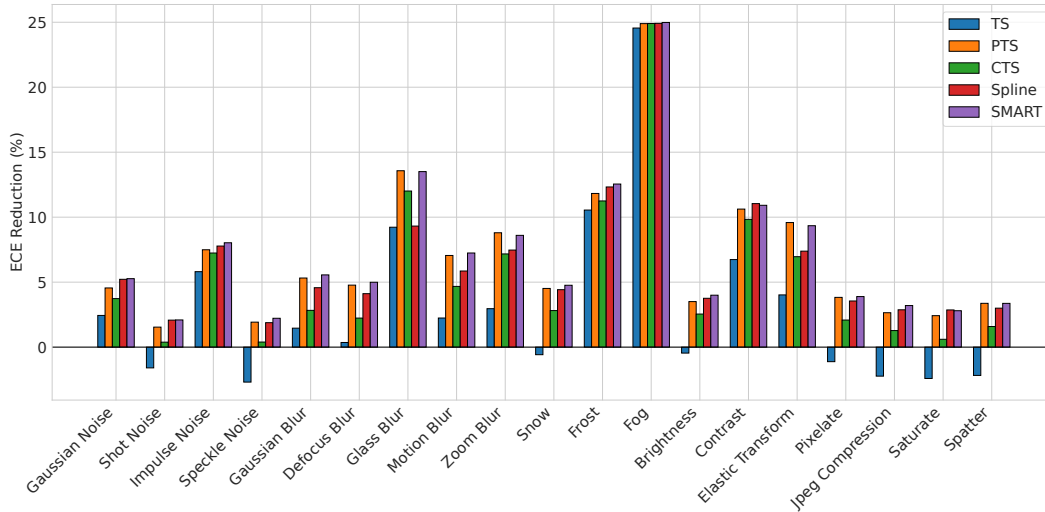


Figure 13: **ECE reduction(↑, %, 15bins) across corruption types for ViT-B/16.** Transformer architectures exhibit distinct calibration challenges under corruption, with global methods often failing while SMART maintains consistent improvements.

showing negative improvements on multiple corruption types including Shot Noise, Speckle Noise, Snow, Brightness, Pixelate, Jpeg Compression, Saturate and Spatter. This demonstrates that transformers’ attention mechanisms and different inductive biases make them fundamentally incompatible with global temperature adjustments under distribution shifts.

SMART maintains consistent positive improvements across all corruption types, though generally more modest than with ResNet-50. This architectural difference suggests that while transformers are inherently better calibrated, they also present unique challenges that require more sophisticated approaches than global scaling. The convergence of all methods on Fog corruption (around 25% improvement) indicates that certain atmospheric corruptions create calibration conditions where architectural differences become less relevant.

A key insight emerges: the logit gap’s decision boundary information remains meaningful across architectures, while global statistics become unreliable for transformers under corruption. PTS

and CTS show more consistent improvements than TS, but SMART’s sample-specific adaptation consistently outperforms all alternatives, confirming its architectural robustness.

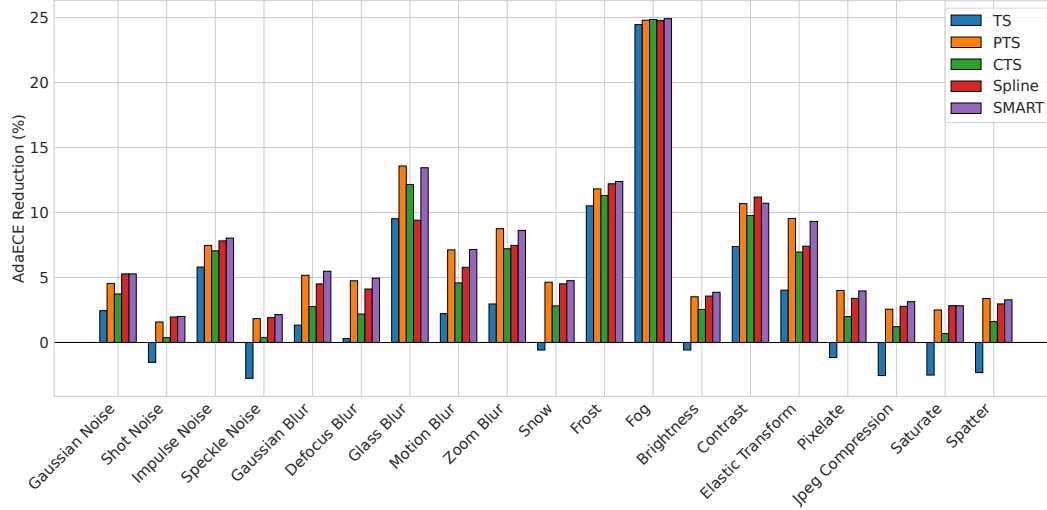


Figure 14: **AdaECE reduction(\uparrow , %, 15bins) across corruption types for ViT-B/16.** Transformer calibration patterns remain consistent under adaptive binning, confirming architectural-specific calibration challenges and SMART’s robustness.

ViT-B/16 AdaECE Analysis The AdaECE results closely replicate the ECE patterns, confirming that transformer calibration behaviors are fundamental architectural characteristics rather than evaluation artifacts. Temperature Scaling’s negative performance persists under adaptive binning, while SMART maintains consistent positive improvements across all corruption types. This metric independence demonstrates that SMART’s logit gap approach captures robust decision boundary information that remains effective regardless of how calibration quality is measured.